Engineering 24 (2023) 73–83

Contents lists available at ScienceDirect

Engineering

journal homepage: www.elsevier.com/locate/eng

Research
Micro and Nano Manipulation and Characterization—Article

Intracellular Strain Evaluation-Based Oocyte Enucleation and Its Application in Robotic Cloning

Ming-Zhu Sun [a,c,#], Yao-Wei Liu [a,c,#], Mao-Sheng Cui [b,*], Qi-Li Zhao [a,c], Xiang-Fei Zhao [a,c], Yi-Di Zhang [a,c], Jing-Jing Huang [b], Gui-Zhang Lu [a], Xin Zhao [a,c,*]

[a] Institute of Robotics and Automatic Information System, Tianjin Key Laboratory of Intelligent Robotics, Nankai University, Tianjin 300071, China
[b] Tianjin Animal Science and Veterinary Research Institute, Tianjin 300201, China
[c] Institute of Intelligence Technology and Robotic Systems, Shenzhen Research Institute of Nankai University, Shenzhen 518063, China

ARTICLE INFO

Article history:
Received 30 July 2021
Revised 25 January 2022
Accepted 25 April 2022
Available online 18 June 2022

Keywords:
Oocyte enucleation
Robotic cloning
Intracellular strain
Intracellular damage
Optical flow

ABSTRACT

Since the first cloned sheep was produced in 1996, cloning has attracted considerable attention because of its great potential in animal breeding. Somatic cell nuclear transfer (SCNT) is widely used for creating clones. However, SCNT is very complicated to manipulate and inevitably causes intracellular damage during manipulation. Typically, only less than 1% of reconstructed embryos develop into live cloned animals. This low success rate is considered to be the major limitation in the extensive application of cloning techniques. In this study, we proposed an intracellular strain evaluation-based oocyte enucleation method to reduce potential intracellular damage in SCNT. We first calculated the intracellular strain based on the intracellular velocity field and then used the intracellular strain as a criterion to improve the enucleation operation. We then developed a robotic batch SCNT system to apply this micromanipulation method to animal cloning. Experimental results showed that we increased the blastocyst rate from 10.0% to 20.8%, and we successfully produced 17 cloned piglets by robotic SCNT for the first time. The success rate of cloning was significantly increased compared to that of traditional methods (2.50% vs 0.73% on average). In addition to the cloning technique, the intracellular strain evaluation-based enucleation method is expected to be applicable to other biological operations and for establishing a universal cell manipulation protocol to reduce intracellular damage.

1. Introduction

Cloning has attracted great attention since Dolly, the first cloned sheep, was produced in 1996 [1] because of its great potential in animal breeding [2–7]. Somatic cell nuclear transfer (SCNT) is a technique for creating clones that involves multiple manipulation procedures, such as oocyte holding; oocyte rotation, penetration, and enucleation; somatic cell aspiration; and injection [8]. However, the efficiency of SCNT is disappointingly low. In Ref. [9], researchers investigated more than 30 experiments on porcine SCNT from 2000 to 2006. The success rate of cloning (number of live offspring per number of embryos transferred) varied; with the average success rate only being 0.73%. For example, in Ref. [10], two sets of donor cells were used to produce 308 nuclear transfer embryos, which were surgically transferred to three surrogate gilts. Five female piglets were delivered by caesarian from one surrogate, resulting in a cloning success rate of 1.6%. In Ref. [11], 2918 nuclear transfer embryos were transferred to 20 recipient gilts, of which three were carried to term, resulting in six live births with a success rate of only 0.21%. Despite recent technological progress, the efficiency has remained largely unchanged since the first cloned animal was delivered [12]. This low success rate has significantly hindered the extensive application of cloning techniques.

Many improvements in SCNT have been made by choosing different cell types [13], changing the cell cycle [14], using different activation and fusion patterns [15,16], transferring different numbers of cloned embryos [17], and so forth. However, relatively less attention has been paid to improving manipulation skills. SCNT is a type of complicated cell surgery, and the level of manipulation skill has a significant influence on cell viability [18]. Thus, improving SCNT manipulation would effectively increase the success rate.

* Corresponding authors.
E-mail addresses: tjsnykxyxmsyyjs@tj.gov.cn (M.S. Cui), zhaoxin@nankai.edu.cn (X. Zhao).
# These authors contributed equally to this work.

https://doi.org/10.1016/j.eng.2022.04.016

Oocyte enucleation, in which genetic materials, including the nucleus and polar body, are extracted from the oocyte using an injection micropipette, is a key step in SCNT. Fig. 1 illustrates the oocyte enucleation process. During enucleation, the cytoplasm is torn rapidly by pressure, and the oocyte loses part of its cytoplasm, leading to huge damage to the oocyte. In previous studies, we designed the path of the injection micropipette inside the oocyte, analyzed the cytoplasm loss for complete removal of the nucleus, and realized enucleation volume control based on the adaptive slide mode [19,20]. These methods reduce cytoplasmic loss and increase developmental potential. However, oocyte enucleation is a complicated dynamic process, and its effect on oocyte viability remains unclear.

During oocyte enucleation, the external force is exerted on the oocyte by the injection micropipette and injector, in which huge deformations of the oocyte are generated, resulting in high intracellular stress. Several force sensors for cell manipulation have recently been reported [21–23], but what the force sensors measured was the stress exerting on the cell. Because intracellular stress cannot be directly measured, we observed the intracellular linear strain instead, which is related to the change in the length of the deformed object [24]. Some physical markers, including fluorescent microbeads [25] and magnetic beads [26], have been applied to intracellular strain measurements. We also proposed a simple and label-free measurement method based on computer vision [27,28].

Several studies have demonstrated that mechanical strain can affect cell viability. Scott confirmed that apoptosis can occur in response to short-term and high-strain mechanical loading [29]; Gladman also revealed that mechanical injury (20% tensile strain) led to significant neuronal cell death [30]. In previous studies, we analyzed the dynamic process of oocyte penetration by evaluating intracellular strain. The experimental results indicate that cellular developmental potential is strongly negatively correlated to intracellular strain [27,28]. Therefore, intracellular strain bridges the cell manipulation and developmental potential. It is important to reduce the intracellular strain during oocyte enucleation to reduce potential intracellular damage.

In this study, we reduced the large intracellular strain by improving enucleation initialization and the dynamic enucleation process. We used a pneumatic injector instead of a conventional hydraulic injector, which is commonly used for manual enucleation. Oocyte enucleation by a hydraulic injector is very fast, but the movement of the cytoplasm is unstable due to oil inertia, leading to a large intracellular strain. As for the pneumatic injector, extra pressure, which is called the balance pressure, is required to balance the capillary force. The initial balance pressure affects the initial force exerted on the oocyte and further affects intracellular strain during enucleation. We evaluated the statistical data on intracellular strain during the entire enucleation process and obtained the proper enucleation initialization parameter.

The dynamic process of cytoplasmic extraction is the most important step in oocyte enucleation. During the process, the force exerted inside the oocyte changes dynamically, leading to large intracellular strain. However, directly performing online enucleation control based on intracellular strain is unrealistic because of the large errors during strain detection. The dynamic strain inside the cell is affected by the change in the pressure of the injector as well as the movement of the cytoplasm. In this paper, we analyzed the relationship between intracellular strain and movement of the cytoplasm in the injection micropipette according to the evaluation results of intracellular strain. We then realized enucleation control via trajectory planning of the cytoplasmic movement to reduce the maximum intracellular strain during this dynamic process.

Finally, we applied the proposed enucleation method to the entire SCNT process and implemented robotic batch SCNT. The experimental results indicated that the proposed oocyte enucleation method reduced the number of large intracellular strains. The maximum strain decreased 60.8% (from 0.79 to 0.31) compared to the manual operation. We then performed SCNT of 113 oocytes using the proposed enucleation method and manual operation. The blastocyst rate, which is the last stage of *in vitro* development of reconstructed embryos and denoting successful cloning, increased from 10.0% to 20.8% when using the proposed method. Finally, we performed SCNT on 525 oocytes using a robotic batch SCNT system. The average success rate and survival rate were 99.1% and 97.1% respectively. A total of 510 embryos were transferred to six recipients. Two recipients became pregnant and delivered ten and seven piglets, respectively. Compared to manual operation, the success rate of cloning increased significantly from an average of 0.73% to 2.50%. We greatly increased the developmental potential by improving the enucleation operation and reducing intracellular strain, achieving robotic cloning results superior to those of manual operation for the first time.

2. Materials and methods

2.1. Intracellular strain calculation in oocyte enucleation

2.1.1. Visual detection in oocyte enucleation

Oocyte enucleation can be divided into two steps according to cytoplasmic movement.

Step 1: Before cytoplasmic movement. The initial balance pressure was set by adjusting the volume of culture medium in the injection micropipette. After micropipette penetration, the pressure was reduced gradually to generate aspiration force until the cytoplasm began to move in the micropipette.

Step 2: Cytoplasmic movement. The cytoplasm was moved into the micropipette from the oocyte by continuously controlling the pressure, as shown in Fig. 1(b).

When enough cytoplasm was aspirated into the injection micropipette, which ensures that the genetic materials have been extracted, the micropipette withdrew from the oocytes separating the cytoplasm inside and outside the micropipette. Simultaneously, the pressure was increased to stop the cytoplasm from moving inside the micropipette, as shown in Fig. 1(c).

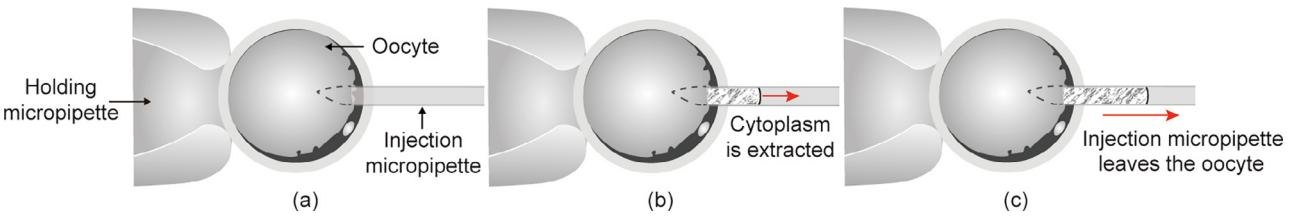

Fig. 1. Oocyte enucleation. (a) Before enucleation, the oocyte is immobilized using the holding micropipette and penetrated by the injection micropipette; (b) during enucleation, the cytoplasm is extracted into the micropipette; (c) after enucleation, the injection micropipette withdraws from the oocyte, while the cytoplasm is still moving inside the micropipette.

In this study, a series of image processing methods were combined to automatically detect the positions of the oocyte, tips of the holding micropipette and injection micropipette, and movement of the cytoplasm in the injection micropipette.

First, we determined the position of holding micropipette region by image scanning and detected the injection micropipette tip outside the oocyte by using a template-matching algorithm. As shown in Fig. 2(a), we set the position of the injection micropipette tip to the middle of the slope of the micropipette tip to facilitate subsequent strain analysis. Second, we obtained the region of interest (ROI) of the oocyte based on the position of the holding micropipette tip. To identify the cell region, we detected the oocyte edge using the Canny edge detection algorithm and found the oocyte contour after open operation of mathematical morphology, as shown in Figs. 2(b)–(d). After the injection micropipette had penetrated the oocyte, we estimated its position according to the distance moved by the micropipette, as shown in Fig. 2(e).

In step 1 of oocyte enucleation, the cytoplasm started to move and entered the micropipette after an aspiration force was exerted on the oocyte for a duration. We used the frame difference method to determine whether the cytoplasm had entered the micropipette. Fig. 3(a) shows the ROI for cytoplasmic movement detection. The difference image was obtained by subtracting two consecutive frames. The difference image was then transformed into a binary image using the Otsu binarization algorithm, as shown in Fig. 3(b). Step 1 was completed when the area of the foreground was greater than the threshold, which was set to 200 pixels in the experiment.

In step 2 of oocyte enucleation, the cytoplasm rapidly moved from the oocyte into the micropipette. We detected the position of the cytoplasmic interface in the micropipette in real time using the Lucas–Kanade optical flow, which is a type of sparse optical flow method [31]. As shown in Fig. 3(c), 100 initial tracking points were selected on the rightmost side of the foreground according to the frame difference result at the end of step 1. The average position of the points on the x-axis was calculated as the initial position of the cytoplasmic interface. Lucas–Kanade optical flow was then applied to cytoplasmic interface tracking, and the average position of the tracking points was calculated frame by frame to update the position of the cytoplasmic interface, as shown in Fig. 3(d). When the cytoplasmic interface moved

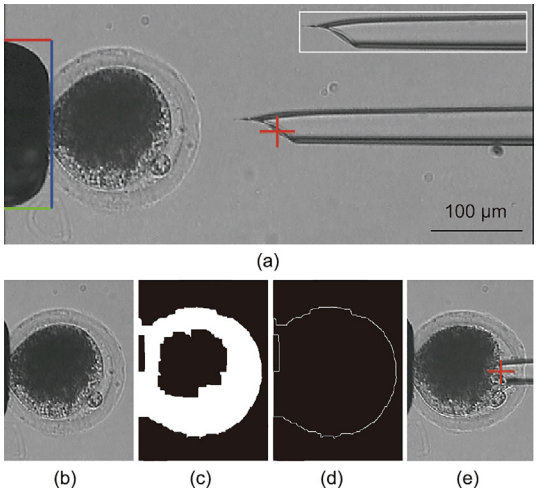

Fig. 2. Visual detection of the micropipettes and the oocyte. (a) Micropipette detection by using image scanning and a template-matching algorithm; (b) region of interest (ROI) of oocyte image; (c) edge detection by the Canny detection algorithm and morphology open operator; (d) oocyte contour by contour detection algorithm; (e) injection micropipette positioning according to the distance moved after the micropipette penetration.

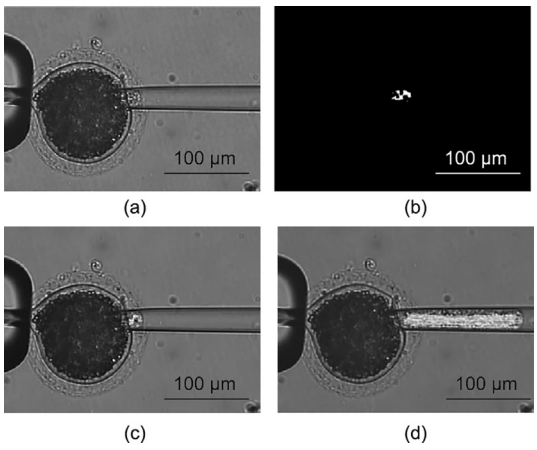

Fig. 3. Visual detection of cytoplasmic movement in oocyte enucleation. (a) ROI for cytoplasmic movement detection; (b) difference image binarization by the Otsu algorithm, step 1 was completed when the area of the foreground was greater than the threshold; (c) tracking point selection according to the frame difference result at the end of step 1; (d) cytoplasmic interface tracking based on Lucas–Kanade optical flow algorithm.

to the set position of the injection micropipette, that is, when sufficient cytoplasm has been aspirated, step 2 was considered complete. Video S1 in Appendix A shows the tracking results of the cytoplasmic interface.

2.1.2. Intracellular strain field calculation based on velocity field

We used the dense optical flow algorithm proposed by Farneback [32] to detect intracellular motion and calculate the intracellular strain field. As shown in Fig. 4(a), we considered a point as an intracellular point every ten pixels in the intracellular region according to the size of the cytoplasmic particles. The velocity field and oocyte deformation of all intracellular points were calculated by applying the optical flow algorithm to two consecutive frames, as shown in Figs. 4(b) and (c). The average error of optical flow detection using forward–backward tracking was 0.67 pixels, which ensured the accuracy of the intracellular strain field calculation. Further, an additional experiment on stretching elastic rubber was conducted to verify the optical flow algorithm. The error was less than 1.00 pixel on average, indicating that the optical flow method can be applied to large deformed objects. (as shown in Fig. S1 and Video S2 in Appendix A).

The intracellular strain fields ε of the oocytes were obtained using Eq. (1):

$$\varepsilon = \lim_{L \to 0} \frac{\Delta L}{L} \tag{1}$$

where L is the initial distance between two adjacent points and ΔL is the distance variation after deformation. During oocyte enucleation, the cytoplasm was transferred into the micropipette and placed perpendicular to the slope of the injection micropipette tip. The deformation of the oocyte as well as the intracellular strain occurred mainly in this direction. We calculated the strain field diagonally at a 45° angle because the micropipette tip is usually opened at a 45° angle for SCNT.

$$\varepsilon = \frac{\sqrt{(x(i+1)-x(i))^2 + (y(i+1)-y(i))^2} - L_0}{L_0} \tag{2}$$

where L_0 is the initial distance between two adjacent intracellular points in one frame; $(x(i), y(i))$ and $(x(i+1), y(i+1))$ are the coordinates of the adjacent points in the next frame, which are calculated using the velocity field of the intracellular points. Fig. 4(d) shows the intracellular strain field. The intracellular structure is stretched

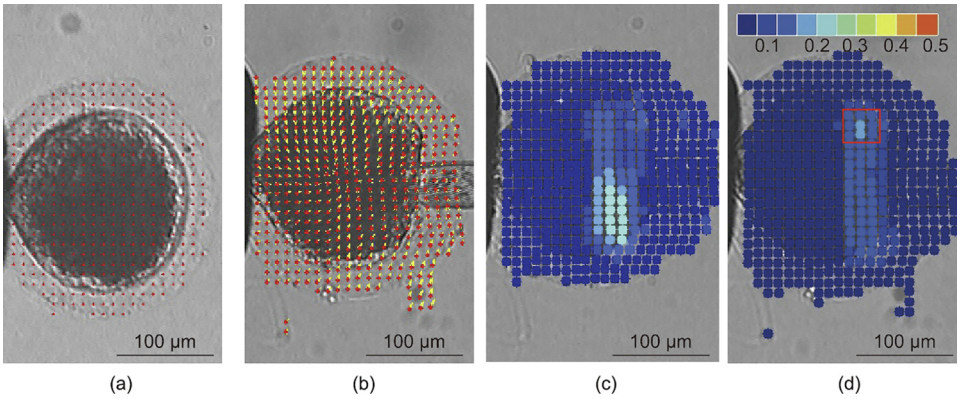

Fig. 4. Calculation of intracellular strain field based on velocity field. (a) Intracellular points (the red points) in the intracellular region; (b) intracellular velocity field (in yellow) in two consecutive frames, the lines with an arrow show the magnitude and direction of the velocities; (c) oocyte deformation in two consecutive frames; (d) intracellular strain field, red and blue represent the high and low values. A 3 × 3 intracellular point region with the largest strain near the micropipette tip was selected as the strain ROI (the red box) for further analysis.

when the strain is greater than zero and compressed when the strain is less than zero. To reduce the large intracellular strain in oocyte enucleation, we selected a 3 × 3 intracellular-point region with the largest strain near the micropipette tip as the strain ROI for further analysis, as shown in the red box in Fig. 4(d).

2.2. Oocyte enucleation based on intracellular strain evaluation

In cell manipulations, a large intracellular strain means a large intracellular deformation; for example, when the values of strain distribution are greater than 0.5, the intracellular structure is stretched by more than a factor of 0.5. Moreover, when cytoplasm is extracted from the oocyte, a high proportion of the negative strain means that oscillation is generated in the oocyte and dominates the enucleation process. Large intracellular deformations and oscillations have an adverse effect on cellular developmental potential. In this study, we analyzed the relationship between enucleation and distribution of the intracellular strain. We then set the initial balance pressure and realized trajectory planning of cytoplasmic movement in the dynamic enucleation process based on intracellular strain evaluation to avoid large intracellular strain and reduce the negative strain.

2.2.1. Enucleation initialization based on intracellular strain evaluation

The initial balance pressure was set before the injection micropipette penetrated the oocytes. Our previous study demonstrated that the balance pressure decreases as more culture media are aspirated into the micropipette [33]. Therefore, we provided different initial balance pressures for enucleation by aspirating different volumes of the culture media into the micropipette. As shown in Fig. 5(a), five typical balance pressures (0.9, 0.8, 0.7, 0.6, and 0.5 psi) (1 psi = 6.895 kPa) were selected as the initial balance pressures, and Fig. 5(b) shows the corresponding positions of the gas–liquid interface (GLI).

Fifty oocytes collected from the same batch were randomly divided into five groups and used for intracellular strain evaluation. The pressure in the injection micropipette continuously decreased from the initial pressure required for enucleation. To ensure consistency, the micropipette was placed in the same position inside the oocyte, and a constant change rate of pressure was maintained. Specifically, during oocyte penetration, the injection micropipette moved horizontally at a speed of 50 $m{\cdot}s^{-1}$ to 3/4 of the oocyte diameter to penetrate the oocyte; the injection micropipette then retracted by 1/2 the oocyte diameter to a suitable position for enucleation. In step 1 of oocyte enucleation, the pressure change rate was set to 0.5 $psi{\cdot}s^{-1}$. Because the pressure decreased rapidly, the cytoplasm was extracted as soon as it was possible to do so. In step 2, the pressure change rate was reduced from 0.5 to 0.1 $psi{\cdot}s^{-1}$ linearly at the maximum acceleration, which decreased the speed of cytoplasmic movement and reduced cytoplasmic loss.

The intracellular strain fields were calculated frame by frame. Fig. 5(c) shows typical strain fields, with the largest intracellular strain occurring during enucleation, indicating that the large values of intracellular strain decrease, and the range shrinks as the initial balance pressure decreases during enucleation.

We obtained a normalized histogram of all intracellular strain values in the strain ROI for each initial balance pressure. Each figure in Fig. 5(d) shows the strain values of 10 enucleation experiments during the entire enucleation process, including steps 1 and 2. Figs. 5(e) and (f) show the percentages of the large intracellular strain distributed in [0.5, 1] and the percentages of the negative intracellular strain with different initial balance pressures, respectively. When the initial balance pressure was high, most strain values were distributed in the positive half-plane of the histogram, which demonstrates that the intracellular structure was under stretch and there was enough driving force for enucleation. However, a large intracellular strain region ([0.5, 1]) was also observed in the histogram, indicating that a large intracellular deformation had been generated. With the decrease in the initial pressure, the large strain region, as well as the large intracellular deformation, decreased, whereas the proportion of the negative strain increased, which means that the oscillation generated in the oocyte and the aspiration force were not large enough to facilitate smooth enucleation. Considering both large strain and negative strain, we set the initial balance pressure to 0.7 psi to avoid large intracellular strain and reduce the negative strain proportion. The intracellular stretch dominated the enucleation process, and the operation could be accomplished with smaller intracellular strain and less oscillation in the oocyte, which may lead to less potential intracellular damage.

2.2.2. Trajectory planning of cytoplasmic interface in injection micropipette

In step 2 of oocyte enucleation, the cytoplasm moves from the oocyte into the micropipette. We divided the enucleation process into multiple periods according to the acceleration variation in the cytoplasmic interface and analyzed the strain distributions in different periods (Fig. S2 in Appendix A). The large intracellular strain is positively correlated with the change in acceleration: the more the acceleration changes, the larger the strain.

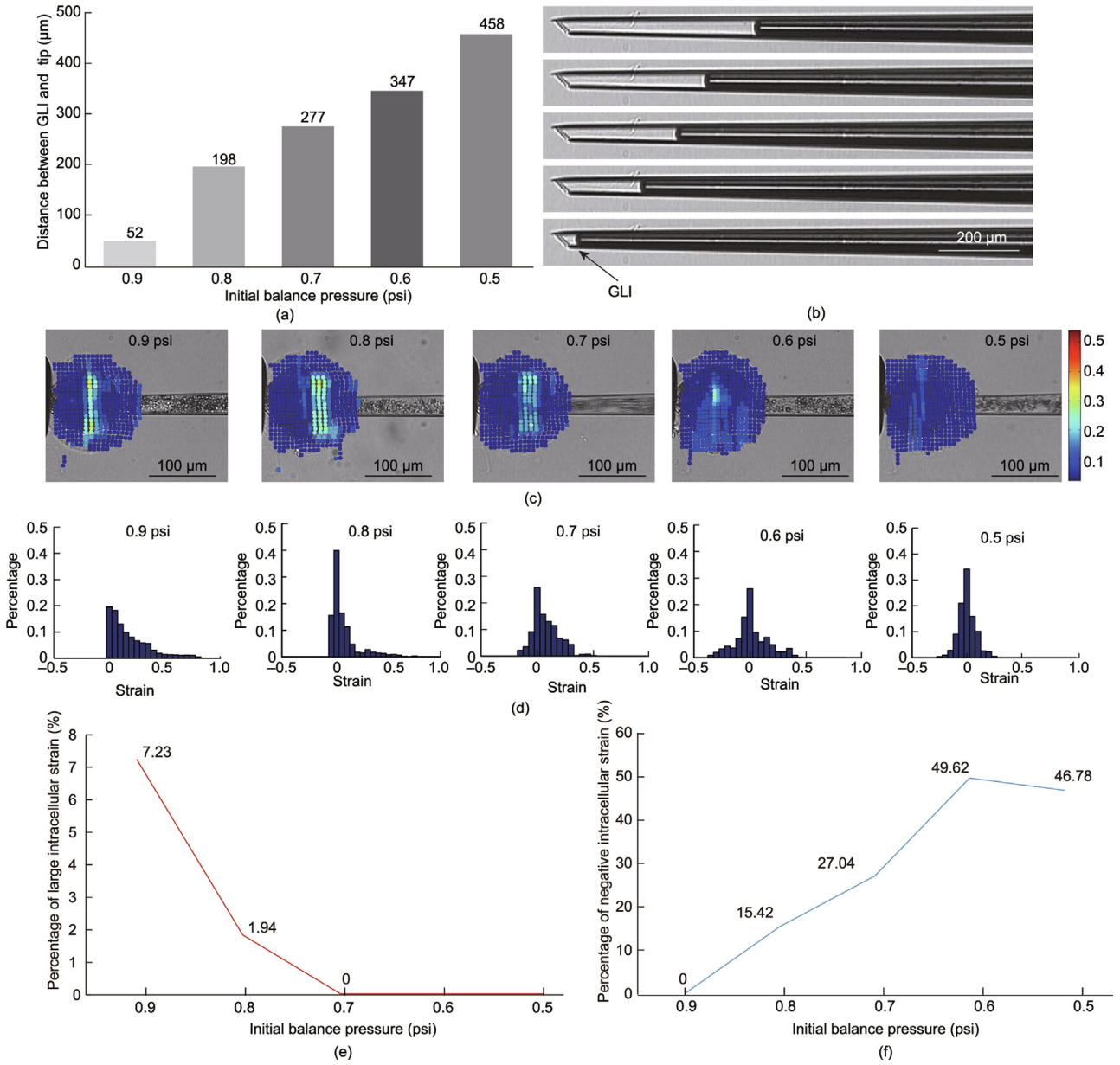

Fig. 5. Intracellular strain with different initial balance pressures. (a) Five typical balance pressures (0.9, 0.8, 0.7, 0.6, and 0.5 psi) by aspirating different volume of culture media; (b) the corresponding positions of gas–liquid interface (GLI) of the initial balance pressures; (c) intracellular strain fields in the enucleation process with different initial balance pressures; (d) normalized histograms of strain values in strain ROI with different initial balance pressures; (e) percentages of the large intracellular strain (strain values distributed in [0.5, 1]) with different initial balance pressures; (f) percentages of negative intracellular strain with different initial balance pressures. 1 psi = 6.895 kPa.

We further selected an enucleation process with an initial balance pressure of 0.7 psi and analyzed the relationship between the intracellular strain and cytoplasmic interface movement. First, we obtained the maximum strain value for each time interval in a given time interval and calculated the standard deviation of the acceleration of the cytoplasmic interface. Second, line fitting was performed during cytoplasmic movement. Because there was a response time from cytoplasmic surface movement to intracellular strain generation, we should analyze the cytoplasmic surface movement corresponding to the intracellular strain with a specific time delay. The optimal delay time was selected based on the goodness of line fitting. Table 1 lists the line-fitting results for different time intervals. A clear linear relationship exists between the maximum strain and the standard deviation of the acceleration of the cytoplasmic interface. The delay time was almost fixed for different time intervals. The fitting result is better when the time interval is larger owing to the strain measurement error. We obtained similar linear fitting results with a time interval of 0.4 s for different initial balance pressures (0.9, 0.8, 0.7, and 0.6 psi), as shown in Fig. 6.

To reduce the large intracellular strain, the variation in the acceleration of the cytoplasmic interface should be limited. To this end, the acceleration of the cytoplasmic interface was set to a constant a_t at time t in step 2 of oocyte enucleation. We assumed that the velocity and acceleration of the cytoplasmic surface were a_0 and v_0 at the end of step 1, which were detected online in the experiment. The acceleration in step 2 increased from the initial acceleration a_0 to a_t in time T_0:

Table 1
Line-fitting of the maximum intracellular strain and standard deviation of the acceleration of the cytoplasmic interface with different time intervals.

Time interval (s)	Optimal delay time (s)	Goodness of line fitting	Slope of the fitted line	Intercept of the fitted line
0.20	0.10	0.9545	0.50	−0.071
0.25	0.08	0.9764	0.51	−0.083
0.30	0.08	0.9783	0.62	−0.095
0.35	0.10	0.9845	0.62	−0.100
0.40	0.08	0.9967	0.68	−0.110

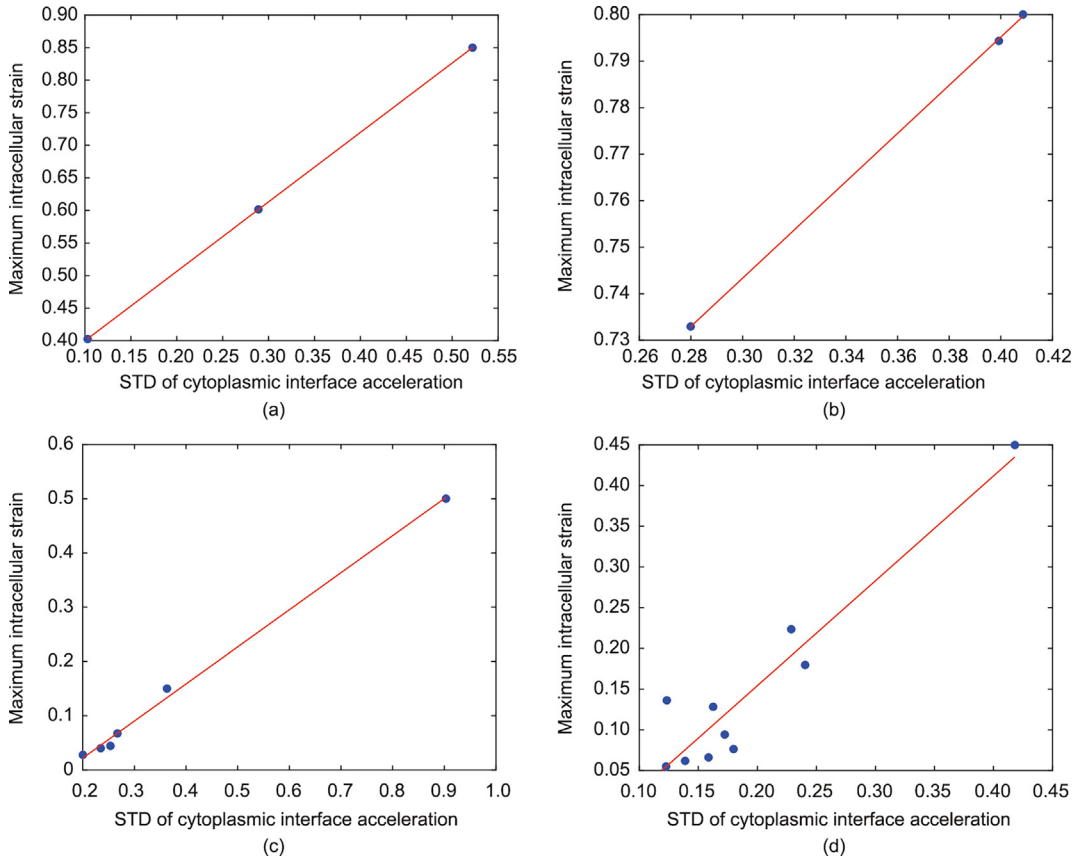

Fig. 6. Linear fitting results with a time interval of 0.4 s for different initial balance pressures. (a) 0.9 psi; (b) 0.8 psi; (c) 0.7 psi; (d) 0.6 psi. STD: standard deviation.

$$a = \begin{cases} a_0 + \dfrac{a_t - a_0}{T_0} t & 0 \le t \le T_0 \\ a_t & T_0 \le t \le T \end{cases} \tag{3}$$

where T is the time of cytoplasmic extraction. The trajectories of the velocity v and displacement S of the cytoplasmic interface can be expressed as follows:

$$v = \begin{cases} v_0 + a_0 t + \dfrac{a_t - a_0}{2T_0} t^2 & 0 \le t \le T_0 \\ v_0 + \dfrac{a_0 - a_t}{2} T_0 + a_t t & T_0 \le t \le T \end{cases} \tag{4}$$

$$S = \begin{cases} v_0 t + \dfrac{a_0}{2} t^2 + \dfrac{a_t - a_0}{6T_0} t^3 & 0 \le t \le T_0 \\ \dfrac{a_t - a_0}{6} T_0^2 + v_0 t + \dfrac{a_0 - a_t}{2} T_0 t + \dfrac{a_t}{2} t^2 & T_0 \le t \le T \end{cases} \tag{5}$$

In these experiments, the movement of the cytoplasmic interface was detected in real time using the Lucas–Kanade optical flow and controlled based on an adaptive slide mode controller [19]. Similar to manual operation, the velocity of the cytoplasm surface was not zero at the end of trajectory planning. Once the cytoplasm interface moved to the set position, the micropipette left the oocytes to stop oocyte enucleation, and the pressure was simultaneously increased.

2.3. Robotic batch SCNT

2.3.1. Robotic SCNT platform

Robotic SCNT was implemented using a self-developed NK-MR601 micromanipulation system, as shown in Fig. 7. It consisted of the following parts: a standard inverted microscope (Olympus, BX-51, Japan) as the basic platform of the system; pair of in-house developed motorized X–Y–Z micromanipulators for positioning the injection micropipette and holding micropipette; an in-house-developed motorized X–Y stage for positioning the petri dish; an in-house-developed pneumatic microinjector for supplying negative aspiration pressure and positive injection pressure; in-house-developed multi-axis controller for motor control; a charge-coupled device (CCD) camera (Panasonic, W-V-460, Japan) for visual detection; and host computer for microscopic image processing, pressure data acquisition, and motion control. The micromanipulators had a travel range of 50 mm × 50 mm ×

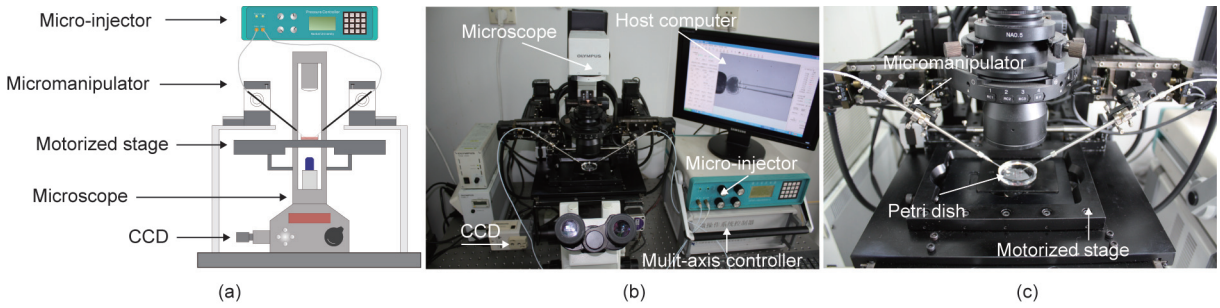

Fig. 7. Self-developed NK-MR601 micromanipulation robotic system for SCNT. (a) Main parts of the micromanipulation system; (b) the Robotic SCNT system; (c) the platform and the micromanipulators. CCD: charge-coupled device.

50 mm, repeatability of 1 μm, and maximum speed of 1 mm·s^{-1}. The *X*–*Y* stage has a travel range of 100 mm × 100 mm, repeatability of 1 μm, and maximum speed of 2 mm·s^{-1}. The pneumatic microinjector has a negative pressure range from −3 to 0 kPa, a resolution of 10 Pa for cell holding, a positive pressure range of 0–200 kPa, and a resolution of 10 Pa for cell injection. The injection valve was connected to a motor to allow the injection pressure to be controlled in real time. All images were captured using ×4 and ×10 objective lenses (Olympus, Japan) with a resolution of 768 × 576 pixels and a frame rate of 20 Hz. In the experiment, the injection micropipette and holding micropipette were assembled on the right and left micromanipulators and connected to the injection channel and holding channel of the micro-injector, respectively.

2.3.2. Robotic batch SCNT procedure

In manual SCNT, the operator finds oocytes and donor cells using the lower objective lens and performs nuclear transfer using the higher objective lens. In the entire SCNT process, the operator converts and focuses the objective lens four times and switches to the different operation areas six times, which is not an efficient method of performing batch SCNT. In robotic SCNT, we designed a global map and obtained a global field of view of the batch oocyte so that batch SCNT could be implemented in an optimized sequence. First, we set up the positions of the five operation areas by human–computer interaction and built a global map in the lower objective lens, as shown in Fig. 8(a). We then obtained the global field of view of the oocyte area by microscopic image stitching and automatically detected the global positions of the oocytes. Finally, the operational order of the oocytes was planned to achieve the shortest path without collision with the micropipettes, as shown in Fig. 8(b).

Furthermore, we divided the robotic SCNT procedure into multiple steps (Fig. S3 in Appendix A) and utilized the oocyte enucleation method based on intracellular strain evaluation in robotic SCNT. First, the initial balance pressure was adjusted to 0.7 psi by aspirating the culture media into the injection micropipette before the micropipette penetrated the oocyte. The pressure was then reduced until the cytoplasm began to move. Second, the cytoplasm, nucleus, and polar body were extracted from the oocyte according to the trajectory planning of the cytoplasmic interface in the injection micropipette. After a sufficient amount of cytoplasm was aspirated, the injection micropipette was withdrawn from the oocyte horizontally at a speed of 100 μm·s^{-1}.

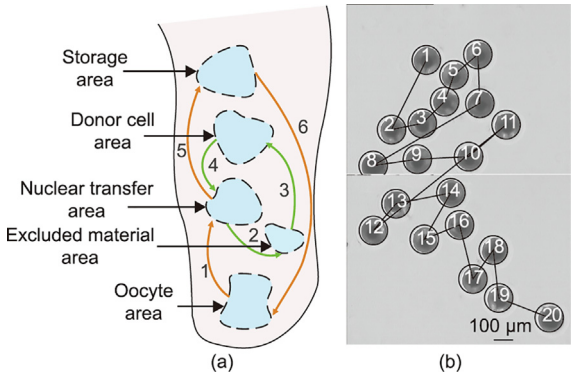

Fig. 8. Global map and the global field of view in robotic batch SCNT. (a) Operation areas and switching order in batch SCNT, we set up the positions of the five operation areas by human–computer interaction and built the global map; (b) global field of view of the oocytes, the figure shows the detection results and the operational order of the oocytes.

3. Results

3.1. Oocyte enucleation control results

According to the enucleation experiment, the time of cytoplasm extraction T was set to 4.0 s, and T_0 was set to 0.2 s in Eqs. (3)–(5). The moving distance of the cytoplasm interface S was set to 150 pixels, considering the cytoplasm loss was set to 8% of the volume of the oocyte for complete removal of the nucleus [20]. The blue line in Fig. 9 shows the desired trajectory of the cytoplasmic interface. In this experiment, the initial velocity and acceleration of the cytoplasmic surface were 20 pixels·s^{-1} and 8 pixels·s^{-2}. The acceleration constant a_t in Eq. (5) was calculated as 8.8 pixels·s^{-2}, and

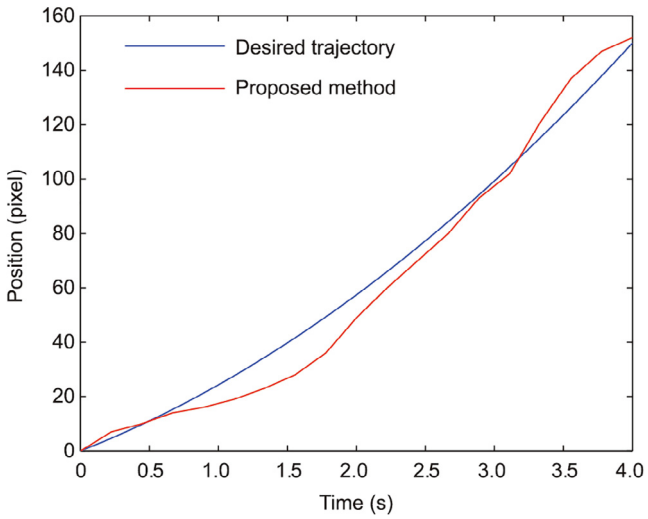

Fig. 9. Trajectory and tracking result of the cytoplasmic interface.

the corresponding standard deviation of the acceleration was 0.1. The movement of the cytoplasmic interface was detected in real time by Lucas–Kanade optical flow with 12 ms per frame. The average detection error was 0.61 pixels. The trajectory of the cytoplasmic surface was tracked using an adaptive slide mode controller [19]. The red line in Fig. 9 indicates the tracking results.

Table 2 shows a comparison of the enucleation methods. Videos S3–S5 in Appendix A show the enucleation processes and strain distributions by manual operation, robotic enucleation method [19], and proposed enucleation method, respectively. The experimental results demonstrate that the enucleation process is more stable when the proposed method is used. The maximum intracellular strain of the proposed method was the smallest. Specifically, the maximum strain was reduced by 60.8% (from 0.79 to 0.31) compared to that in the typical manual operation with an initial balance pressure of 0.9 psi.

3.2. Robotic batch SCNT results

There are two main parts of robotic batch SCNT. First, the global map was built under the lower objective lens (×4), and then the oocytes were individually manipulated under the higher objective lens (×10), as shown in Video S6 in Appendix A. The process for each SCNT is as follows. Fig. 10 shows the manipulation results.

(1) Move the holding micropipette and the injection micropipette to the field of view, and then move the oocyte to the center of the field of view after oocyte relocalization. Fig. 10(a) shows the localization results of the micropipettes and oocyte.

(2) Hold the oocyte using a holding micropipette and rotate the oocyte along the *Y*-axis and *Z*-axis until the polar body points to the desired orientation. We derived the minimum force for oocyte rotation to ensure minimum deformation of the oocyte [34], and Fig. 10(b) shows the oocyte holding and rotation results (polar body at 4 o'clock).

(3) Adjust the initial balance pressure to 0.7 psi for oocyte enucleation, penetrate the oocyte using the injection micropipette, and move the micropipette tip to the same position in the oocyte; Fig. 10(c) shows that the oocyte has been penetrated.

(4) Reduce the balance pressure rapidly after the GLI is stable and until the cytoplasm starts to move, as shown in Fig. 10(d).

(5) Adjust the balance pressure and extract the cytoplasm, as well as the nucleus and the polar body, from the oocyte according to the trajectory planning result of the cytoplasmic interface in the injection micropipette, as shown in Fig. 10(e).

(6) Withdraw the injection micropipette from the oocyte. Fig. 10(f) shows the end of enucleation.

(7) Exclude the genetic materials from the injection micropipette, as shown in Fig. 10(g).

(8) Select a proper donor cell, and aspirate the donor cell into the injection micropipette. Fig. 10(h) shows the donor cell in the micropipette.

(9) Inject the donor cell into the oocyte. Fig. 10(i) shows the donor cell injection result.

Table 2
Enucleation method comparison.

Methods	Initial balance pressure (psi)	Maximum strain
Manual operation	0.9	0.79
	0.7	0.49
Robotic enucleation method [19]	0.7	0.46
Proposed method	0.7	0.31

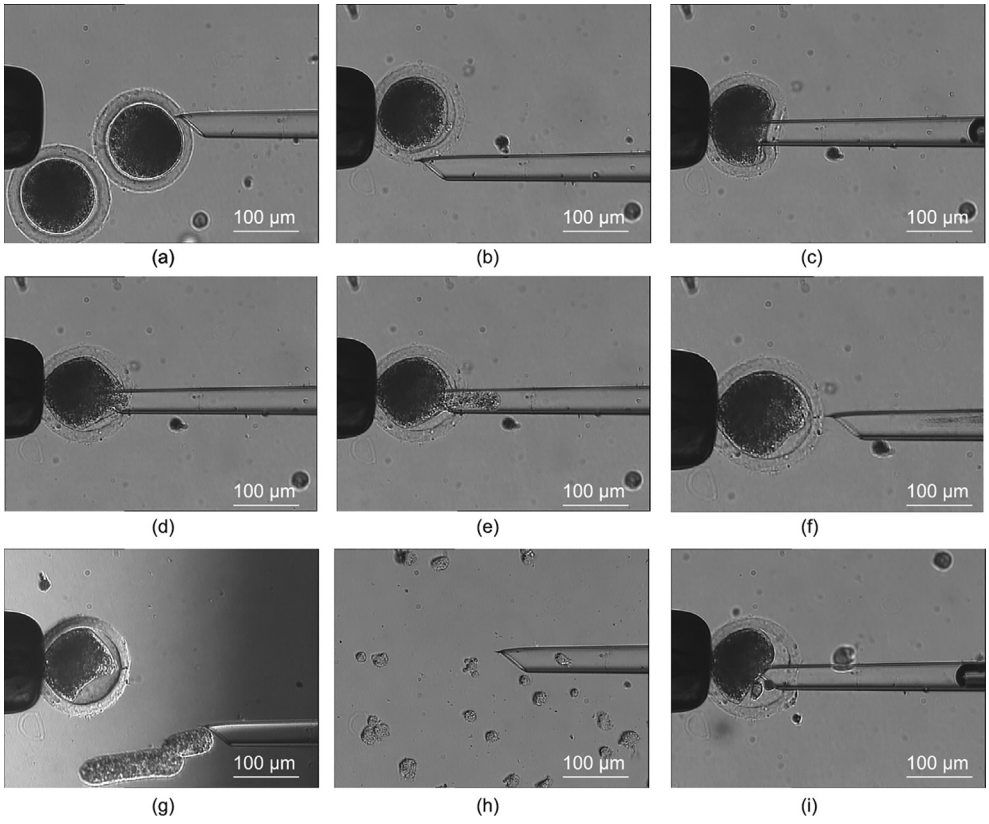

Fig. 10. Robotic SCNT procedure. (a) Micropipettes and oocyte localization; (b) oocyte holding and rotation to the desired orientation (polar body at 4 o'clock); (c) oocyte penetration after enucleation initialization; (d) balance pressure reducing, until the cytoplasm starts to move; (e) the cytoplasm, as well as the nucleus and the polar body, was extracted from the oocyte; (f) end of enucleation; (g) genetic material exclusion; (h) donor cell aspiration; (i) donor cell injection.

In robotic batch SCNT, we need not convert the objective lens and halve the number of objective lens focusing using the robotic system based on the global field of view. Taking a group of 20 oocytes as an example, we spent approximately 21 s building the global map, but we reduced the objective lens conversion and objective lens focusing 40 and 20 folds, respectively. For each SCNT, it took approximately 86 s to manipulate one oocyte. Table 3 lists the time spent on the key steps. It took 1741 s to manipulate a group of 20 oocytes, which means that the operation speed was approximately 87 s per cell.

To verify the effect of the enucleation method on the cellular developmental potential, we performed batch SCNT on 113 oocytes using the proposed method and manual operation. In the proposed method, the initial balance pressure was set to 0.7 psi. The cytoplasm, nucleus, and polar body were extracted from the oocyte according to the trajectory planning results of the cytoplasmic interface in the injection micropipette. The maximum intracellular strain produced during this process was 0.31. In manual operation, the initial balance pressure was set at 0.9 psi to ensure the GLI in the field of view, which is convenient for the operator. The maximum intracellular strain during the manual enucleation process was 0.79.

The operated oocytes, which were restructured embryos, were activated and cultured for seven days. It is 11 out of 53 embryos that developed into blastocysts when the proposed method was applied; in contrast, 6 out of 60 embryos developed into blastocysts via the manual operation. The blastocyst rate increased from 10.0% to 20.8% when using the proposed method, demonstrating that large intracellular strain would cause damage to cell development and affect cellular developmental potential. This is a great achievement because blastocysts are the last stage of the *in vitro* development of reconstructed embryos and are a symbol of successful cloning.

3.3. Pig cloning by robotic SCNT

We performed SCNT from six groups of 525 oocytes using the robotic system, in which 520 oocytes were operated successfully and activated for transfer, and 510 oocytes developed into embryos. Table 4 shows the results of the robotic SCNT and those of pig cloning. The average success rate and survival rate were 99.1% and 97.1%, respectively. Subsequently, 510 embryos were transferred to six recipients. Two recipients were pregnant (Fig. S4 in Appendix A). Ten piglets were delivered by one recipient (No. 206) on day 103 of gestation, consisting of seven healthy piglets and three weak piglets. Three weak piglets died 2–3 days later. The average birth weight of the piglets was 1.32 kg (range 1.25–1.46 kg). Seven piglets were delivered by another recipient (No. 14304) on day 110 of gestation, consisting of six healthy piglets and one weak piglet. The weak piglet died 29 days later. The average birth weight was 1.62 kg (range 1.51–1.85 kg). We increased the success rate of pig cloning from 0.73% for manual operation to an average to 2.5% (13/510). Fig. 11 shows 13 healthy piglets at 90 and 93 days of age.

We performed microsatellite analysis of the genomic DNA from each sample (Table S1 in Appendix A). The comparison results indicated that 13 of the nuclear transfer piglets were derived from the donor cell line B301 with 100% identity for all eight microsatellite markers. All nuclear transfer piglets were significantly different from the surrogate mothers (No. 206 and No. 14304). See the Materials and Methods section in Appendix A for more details.

Table 3
Operation time of robotic SCNT.

Step	Operation time (s)	
	One oocyte	A group (20 oocytes)
Global map building	—	21
Localization	1	20
Oocyte holding and rotation	26	520
Oocyte penetration and enucleation	9	180
Donor cell aspiration and injection	43	860
Oocyte release	7	140
Total	86	1741

4. Discussion

In this study, we analyzed the process of oocyte enucleation in detail and developed an intracellular strain evaluation-based oocyte enucleation method. Because intracellular strain bridges cell manipulation and cellular developmental potential, we improved the enucleation operation to reduce large intracellular strain, as well as the potential intracellular damage during oocyte enucleation. We evaluated the statistical data of intracellular strain during the entire process of enucleation and obtained a reasonable enucleation initialization parameter, the initial balance pressure for enucleation. Further, we analyzed the relationship between the intracellular strain and cytoplasmic movement in the dynamic process of enucleation and designed the trajectory of the cytoplasmic movement in the injection micropipette according to the evaluation of the intracellular strain. The experimental results indicate that the proposed method markedly reduces large intracellular strains. The maximum strain decreased 60.8% (from 0.79 to 0.31), compared with the manual operation with initial balance pressure of 0.9 psi.

Fig. 11. Thirteen healthy piglets produced by robotic SCNT.

Table 4
Robotic SCNT results and cloned pig results.

Experiment Group	Number of operated oocytes	Number of activated oocytes	Number of transplanted oocytes	Success rate (%)	Survival rate (%)	Pregnancy condition	Number of natal pigs	Number of healthy pigs
1	103	102	100	99.0	97.1	Yes	10	7
2	115	113	110	98.3	95.7	Yes	7	6
3	83	82	80	98.8	96.4	No	—	—
4	81	81	80	100.0	98.8	No	—	—
5	71	70	70	98.6	98.6	No	—	—
6	72	72	70	100.0	97.2	No	—	—
Total	525	520	510	99.1	97.1	2	17	13

Furthermore, we evaluated the developmental potential of the oocytes after enucleation. Reconstructed embryos developed into blastocysts after nuclear transfer. We increased the blastocyst rate from 10.0% to 20.8% using the proposed method, which is a great achievement because blastocyst is the symbol of successful cloning.

Finally, we applied the oocyte enucleation method to SCNT and implemented a robotic-batch SCNT system. There 17 cloned piglets were successfully produced, and 13 clones developed to term with a cloning success rate of 2.5%, achieving operation results superior to those of manual operation for the first time. Robotic SCNT ensures consistent manipulation and operation results, from which biochemistry operation environments and conditions in the cloning process can benefit the most.

The higher developmental potential implies that the proposed method reduces intracellular damage during the manipulation process. Several studies have evaluated intracellular damage at the cellular level. For example, cell mechanical damage caused by microinjection can be analyzed by counting the number of ruptured bonds [35] or evaluating the intracellular damage caused by chilling injury based on fluorescent staining [36]. However, the mechanism of the intracellular damage caused by micromanipulation remains unclear. Our study provides an experimental platform to explore the mechanism of intracellular damage and an approach to reduce damage.

From the perspective of the objects to be operated, we introduced intracellular strain into micromanipulation and provided an approach to achieve operation results superior to those of manual operation. This will promote cloning technology applications and many other biological operations, such as intracytoplasmic sperm injection and polar-body genome transfer. Robotic systems for biological manipulations, such as surgical robots, also cause biological damage to tissues and organs. However, it is difficult to evaluate the damage due to the complexity of the organisms. In this study, we explored the connection between robotic manipulations, intracellular strain, and potential intracellular damage at the cellular level, which also opens a door to exploring the damage during manipulations of surgical robots.

In the future, we will further improve robotic SCNT. However, oocyte rotation and donor cell aspiration take a long time, as shown in Table 3. We will design new oocyte rotation and cell aspiration methods based on kinematic modeling and fluid modeling to improve operation efficiency. In addition, we will analyze the geometric and mechanical properties of oocytes and expand the robotic SCNT to other animals, such as mice and sheep.

Acknowledgments

This research was jointly supported by the National Key Research and Development Program of China (2018YFB1304905), the National Natural Science Foundation of China (NSFC) (62027812, U1813210, 62003174, and 61903201), and China Postdoctoral Science Foundation (2020M680865). We thank Professor Li-Ning Sun and Professor Jin-Chang Liu for helpful discussions and suggestions.

Compliance with ethic guidelines

Ming-Zhu Sun, Yao-Wei Liu, Mao-Sheng Cui, Qi-Li Zhao, Xiang-Fei Zhao, Yi-Di Zhang, Jing-Jing Huang, Gui-Zhang Lu, and Xin Zhao declare that they have no conflict of interest or financial conflicts to disclose.

Appendix A. Supplementary data

Supplementary data to this article can be found online at https://doi.org/10.1016/j.eng.2022.04.016.

References

[1] Campbell KHS, McWhir J, Ritchie WA, Wilmut I. Sheep cloned by nuclear transfer from a cultured cell line. Nature 1996;380(6569):64–6.
[2] Baguisi A, Behboodi E, Melican DT, Pollock JS, Destrempes MM, Cammuso C, et al. Production of goats by somatic cell nuclear transfer. Nat Biotechnol 1999;17(5):456–61.
[3] Polejaeva IA, Chen SH, Vaught TD, Page RL, Mullins J, Ball S, et al. Cloned pigs produced by nuclear transfer from adult somatic cells. Nature 2000;407(6800):86–90.
[4] Chesné P, Adenot PG, Viglietta C, Baratte M, Boulanger L, Renard JP. Cloned rabbits produced by nuclear transfer from adult somatic cells. Nat Biotechnol 2002;20(4):366–9.
[5] Lee BC, Kim MK, Jang G, Oh HJ, Yuda F, Kim HJ, et al. Dogs cloned from adult somatic cells. Nature 2005;436(7051):641.
[6] Kuwayama H, Tanabe Y, Wakayama T, Kishigami S. Birth of cloned mice from vaginal smear cells after somatic cell nuclear transfer. Theriogenology 2017;94:79–85.
[7] Liu Z, Cai Y, Wang Y, Nie Y, Zhang C, Xu Y, et al. Cloning of macaque monkeys by somatic cell nuclear transfer. Cell 2018;172(4):881–7.
[8] Akagi S, Matsukawa K, Takahashi S. Factors affecting the development of somatic cell nuclear transfer embryos in cattle. J Reprod Dev 2014;60(5):329–35.
[9] Vajta G, Zhang Y, Macháty Z. Somatic cell nuclear transfer in pigs: recent achievements and future possibilities. Reprod Fertil Dev 2007;19(2):403–23.
[10] Park KW, Cheong HT, Lai L, Im GS, Kühholzer B, Bonk A, et al. Production of nuclear transfer-derived swine that express the enhanced green fluorescent protein. Anim Biotechnol 2001;12(2):173–81.
[11] Ramsoondar JJ, Macháty Z, Costa C, Williams BL, Fodor WL, Bondioli KR. Production of α1,3-galactosyltransferase-knockout cloned pigs expressing human α1,2-fucosylosyltransferase. Biol Reprod 2003;69(2):437–45.
[12] Czernik M, Anzalone DA, Palazzese L, Oikawa M, Loi P. Somatic cell nuclear transfer: failures, successes and the challenges ahead. Int J Dev Biol 2019;63:123–30.
[13] Inoue K, Ogonuki N, Mochida K, Yamamoto Y, Takano K, Kohda T, et al. Effects of donor cell type and genotype on the efficiency of mouse somatic cell cloning. Biol Reprod 2003;69(4):1394–400.
[14] Kato Y, Tsunoda Y. Role of the donor nuclei in cloning efficiency: can the ooplasm reprogram any nucleus? Int J Dev Biol 2010;54(11–12):1623–9.
[15] Choi JY, Kim CI, Park CK, Yang BK, Cheong HT. Effect of activation time on the nuclear remodeling and *in vitro* development of nuclear transfer embryos derived from bovine somatic cells. Mol Reprod Dev 2004;69(3):289–95.
[16] Aston KI, Li GP, Hicks BA, Sessions BR, Pate BJ, Hammon D, et al. Effect of the time interval between fusion and activation on nuclear state and development *in vitro* and *in vivo* of bovine somatic cell nuclear transfer embryos. Reproduction 2006;131(1):45–51.
[17] Li Z, Shi J, Liu D, Zhou R, Zeng H, Zhou X, et al. Effects of donor fibroblast cell type and transferred cloned embryo number on the efficiency of pig cloning. Cell Reprogram 2013;15(1):35–42.
[18] Lu Z, Zhang X, Leung C, Esfandiari N, Casper RF, Sun Y. Robotic ICSI (intracytoplasmic sperm injection). IEEE Trans Biomed Eng 2011;58(7):2102–8.
[19] Zhao X, Cui M, Zhang Y, Liu Y, Zhao X. Robotic precisely oocyte blind enucleation method. Appl Sci 2021;11(4):1850.
[20] Zhao Q, Qiu J, Feng Z, Du Y, Liu Y, Zhao Z, et al. Robotic label-free precise oocyte enucleation for improving developmental competence of cloned embryos. IEEE Trans Biomed Eng 2021;68(8):2348–59.
[21] Wang G, Xu Q. Design and precision position/force control of a piezo-driven microinjection system. IEEE/ASME Trans Mechatron 2017;22(4):1744–54.
[22] Mohand-Ousaid A, Haliyo S, Régnier S, Hayward V. High fidelity force feedback facilitates manual injection in biological samples. IEEE Robot Autom Lett 2020;5(2):1758–63.
[23] Wei Y, Xu Q. Design and testing of a new force-sensing cell microinjector based on small-stiffness compliant mechanism. IEEE/ASME Trans Mechatron 2021;26(2):818–29.
[24] Marrett R, Peacock DCP. Strain and stress. J Struct Geol 1999;21(8–9):1057–63.
[25] Barbee KA, Thibault LE. Strain measurements in vascular smooth muscle cells grown on a biaxially-stretched substrate. In: Proceedings of the Annual International Engineering in Medicine and Biology Society; 1989 Nov 9–12; Seattle, WA, USA. IEEE; 1989. p. 864–5.
[26] Bonakdar N, Gerum R, Kuhn M, Spörrer M, Lippert A, Schneider W, et al. Mechanical plasticity of cells. Nat Mater 2016;15(10):1090–4.
[27] Sun Y, Liu Y, Zhao Q, Sun M, Zhao X. Modeling and measuring intracellular displacement during cell penetration. J Appl Phys 2020;127(4):044701.
[28] Liu Y, Cui M, Sun Y, Feng Z, Bai Y, Sun M, et al. Oocyte orientation selection method based on the minimum strain position in the penetration process. J Appl Phys 2019;125(15):154701.

[29] Scott A, Khan KM, Heer J, Cook JL, Lian O, Duronio V. High strain mechanical loading rapidly induces tendon apoptosis: an *ex vivo* rat tibialis anterior model. Br J Sports Med 2005;39(5):e25.
[30] Gladman SJ, Ward RE, Michael-Titus AT, Knight MM, Priestley JV. The effect of mechanical strain or hypoxia on cell death in subpopulations of rat dorsal root ganglion neurons *in vitro*. Neuroscience 2010;171(2):577–87.
[31] Lucas BD, Kanade T. An iterative image registration technique with an application to stereo vision. In: Proceedings of the 7th International Joint Conference on Artificial Intelligence (IJCAI); 1981 Aug 24–28; Vancouver, BC, Canada. IJCAI; 1981. p. 674–9.
[32] Farneback G. Very high accuracy velocity estimation using orientation tensors, parametric motion, and simultaneous segmentation of the motion field. In: Proceedings of the Eighth IEEE International Conference on Computer Vision (ICCV 2001); 2001 Jul 7–14; Vancouver, BC, Canada. IEEE; 2001. p. 171–7.
[33] Zhao Q, Wu M, Cui M, Qin Y, Yu J, Sun M, et al. A novel pneumatic micropipette aspiration method using a balance pressure model. Rev Sci Instrum 2013; 84(12):123703.
[34] Zhao Q, Sun M, Cui M, Yu J, Qin Y, Zhao X. Robotic cell rotation based on the minimum rotation force. IEEE Trans Autom Sci Eng 2015;12 (4):1504–15.
[35] Liu F, Wu D, Wu X, Chen K. Analyses of the cell mechanical damage during microinjection. Soft Matter 2015;11(7):1434–42.
[36] Zeron Y, Pearl M, Borochov A, Arav A. Kinetic and temporal factors influence chilling injury to germinal vesicle and mature bovine oocytes. Cryobiology 1999;38(1):35–42.